Direct Observation of Spatiotemporal Dynamics of Short Electron Bunches in Storage Rings

C. Evain,[1,*] E. Roussel,[2] M. Le Parquier,[1] C. Szwaj,[1] M.-A. Tordeux,[3] J.-B. Brubach,[3] L. Manceron,[3] P. Roy,[3] and S. Bielawski[1]

[1]*Laboratoire de Physique des Lasers, Atomes et Molécules, UMR CNRS 8523 Centre d'Études et de Recherches Lasers et Applications, FR CNRS 2416, Université des Sciences et Technologies de Lille, F-59655 Villeneuve d'Ascq Cedex, France*

[2]*Elettra-Sincrotrone Trieste, Strada Statale 14-km 163,5 in AREA Science Park,34149 Basovizza, Trieste, Italy*

[3]*Synchrotron SOLEIL, Saint Aubin, BP 34, 91192 Gif-sur-Yvette, France*

(Received 28 July 2016; published 2 February 2017)

In recent synchrotron radiation facilities, the use of short (picosecond) electron bunches is a powerful method for producing giant pulses of terahertz coherent synchrotron radiation. Here we report on the first direct observation of these pulse shapes with a few picoseconds resolution, and of their dynamics over a long time. We thus confirm in a very direct way the theories predicting an interplay between two physical processes. Below a critical bunch charge, we observe a train of identical THz pulses (a broadband Terahertz comb) stemming from the shortness of the electron bunches. Above this threshold, a large part of the emission is dominated by drifting structures, which appear through spontaneous self-organization. These challenging single-shot THz recordings are made possible by using a recently developed photonic time stretch detector with a high sensitivity. The experiment has been realized at the SOLEIL storage ring.

DOI: 10.1103/PhysRevLett.118.054801

In last generation storage ring facilities, it has become possible to produce pulses of coherent synchrotron radiation (CSR), with powers that exceed classical (incoherent) synchrotron radiation by factors greater than 10 000 [1–7], and may be organized in Terahertz combs [8,9].

A privileged way for obtaining this type of emission with the stability required for users, consists of operating the storage ring facilities with short (picosecond) electron bunches [2,6,7,10–14]. As the main idea, if the longitudinal shape of an electron bunch presents Fourier components at terahertz frequencies, an intense and stable emission of coherent terahertz radiation is generally expected in bending magnets of accelerators, as illustrated in Fig. 1.

This simple conceptual picture is nevertheless deeply complicated by a physical phenomenon of very fundamental nature: the interaction of electron bunches with their own emitted radiation leads to a spatiotemporal instability, which is characterized by the spontaneous appearance of microstructures at the millimeter scale [16–18]. In turn, these structures also emit CSR. Hence, the interplay between these two modes of emission (i.e., from the "shortness" of the electron bunches and from the spontaneously formed microstructures) plays a central role in the knowledge and improvement of the present and future CSR sources.

However, it is only recently that direct experimental observation of the emitted THz electric field pulse shapes became possible. As an important milestone, electro-optic sampling has become possible in storage rings either for recording CSR pulses [19,20], and electron bunch near-field shapes [21]. Then the so-called photonic time-stretch strategy [22,23] opened the way to direct recordings of CSR electric field pulse shapes, over successive shots at ultrahigh repetition rates [24] (see also Refs. [25–27] for other photonic-hardware acceleration strategies).

Nevertheless, the limited sensitivity of these new high-repetition-rate picosecond detectors limited experimental investigation of THz signals to special conditions of high bunch charge and long electron bunches. This configuration corresponds to the highest possible peak powers, but also to strongly unstable operation [18,24]. Thus, characterization of CSR pulse shape dynamics remained an open question for short (picosecond scale) and low-charge electron bunches, i.e., the specific conditions where exploiting this fundamental phenomenon, as a THz source, are foreseen.

In this Letter, we present the actual shapes (the electric field evolution, including envelope and carrier) of the THz CSR pulses emitted in short bunch operation in a storage ring. This analysis has been possible by combining two recent advances in terahertz electric field detection: high-sensitivity electro-optic sampling [15,28] for obtaining the required signal-to-noise ratio with picosecond resolution, and the so-called time-stretch strategy [22–24], which enables single-shot recordings at ultrahigh acquisition rates. As a main result, we present a direct characterization of the transition from stable terahertz emission to dynamically evolving pulses: the microbunching instablity threshold, which plays a central role in theories of CSR [16,17,29]. We also show that numerical integration of the Vlasov-Fokker-Planck equation reproduces the main characteristics of the experimental signals.

The experiment has been performed at the SOLEIL storage ring in a so-called *low-alpha* user shift. This mode

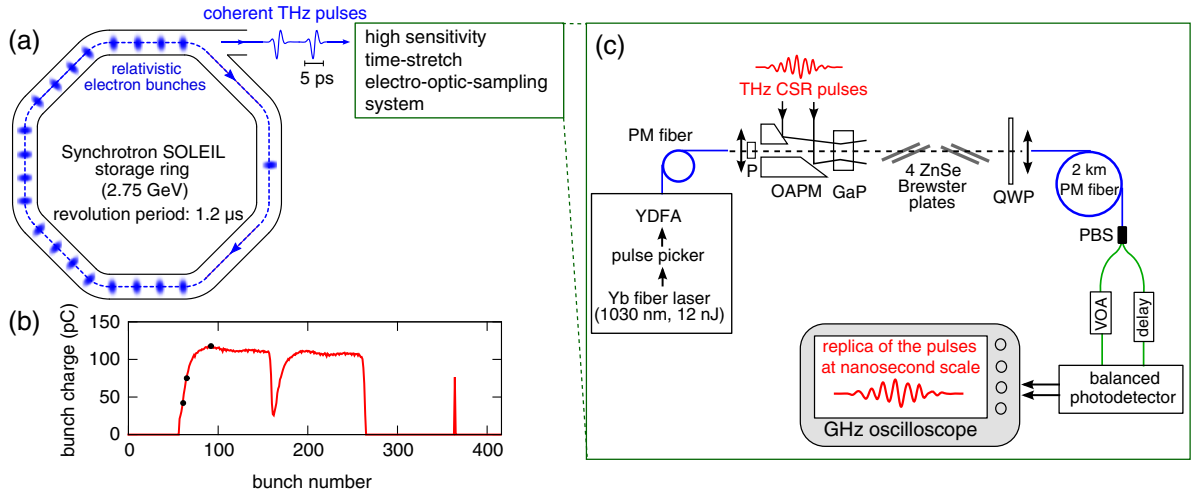

FIG. 1. (a) Global experimental arrangement. The SOLEIL storage ring is operated with many short electron bunches (209 in the experiment: 208 successive bunches and one isolated bunch). The THz coherent synchrotron radiation pulses emitted in a bending magnet are recorded in single shot with picosecond resolution at the THz/IR AILES beam line, using high-sensitivity photonic time-stretch electro-optics sampling. (b) Distribution of the electron bunch charges over one turn for this experiment. The three dots indicate the electron bunches whose CSR pulse evolutions are displayed in Figs. 2 and 3. (c) Photonic time stretch electro-optical sampling setup. Blue lines are polarization-maintaining (PM) fibers (PM980). Green lines are single mode fibers (HI1060). Fibered polarizing beam splitter (PBS), off-axis parabolic mirror (OAPM), polarizer (P), 5 mm long, [110]-cut gallium phosphide crystal (GaP), quarter-wave plate (QWP), variable optical attenuator (VOA), and adjustable delay line (delay). The balanced detector is an DCS-R412 from discovery semiconductors. The use of the four ZnSe plates enables us to enhance the setup detectivity (see text and Ref. [15]). The polarizations of the laser and THz field are parallel and oriented along the $[-110]$ axis of the GaP crystal (and peremptory to the figure plane). The QWP is adjusted at 45° with respect to the laser polarization.

is characterized by the operation of short bunches (of about 5 ps rms [30]), which emit CSR with a stability which is compatible with THz user experiments. Moreover the 209 bunches, which circulate in the storage ring have typically different charges [Fig. 1(b)]. This allows investigations as a function of bunch charge by simply studying the emission of each individual electron bunch, without change of the storage ring operating conditions.

The THz CSR pulses are recorded on the AILES beam line, using a photonic time-stretch electro-optic sampling setup, which is specially designed for high sensitivity [Fig. 1(c)]. This detection system is composed of two parts, which are partly intertwined (see also Ref. [31] for details). The first part is a single-shot EOS [32,33] system based on the design developped at SLS [20], FLASH [34], and ANKA [21], which imprints the THz electric evolution onto the longitudinal profile of a chirped laser pulse at 1030 nm. As a key point for reaching the required high sensitivity, we follow the special strategy recently published by Ahmed, Savolainen, and Hamm [15,28], which consists of using balanced detection, and introducing a set of Brewster plates as shown in Fig. 1(c). In order to obtain the necessary high acquisition rates, we associated this EOS setup with the so-called photonic time stretch technique developed by B. Jalali and co-workers [22,35]. The chirped laser pulses containing the THz pulse shape information are stretched within a 2 km-long fiber [23], up to the nanosecond scale. At the balanced photodetectors output, we thus obtain a "replica" of CSR pulse, that is temporally magnified, by a factor of about 200. The optical performances of the setup are described in detail in Ref. [31]. The acquisition window is of the order of 15 ps, and the sensitivity is of 2.3 $\mu V/cm/\sqrt{Hz}$ at 300 GHz in the electro-optic crystal (i.e., 1.25 V/cm over the 0–300 GHz band). Since the frequency range of the CSR pulses is typically in the 150–600 GHz range [6,14], the stretched signal to be recorded by the oscilloscope is in the 0.75–3 GHz range. Here we use a Teledyne LeCroy LabMaster 10–65Zi oscilloscope (with an—overdimensioned—30 GHz bandwidth), and the acquired data are numerically low-pass filtered at 6 GHz. We recorded a 3 ms-long time series, which corresponds to approximately 2500 turns in the storage ring. Typical single-shot recordings of the THz CSR pulses (electric field vs time) are represented in Fig. 2. In order to obtain a synthetic view of the CSR pulse dynamics over a large number of turns in the storage ring, we also represented the pulse series in a color scale diagram, versus time and number of turns, as displayed in Figs. 3(a)–3(c), for three values of bunch charge.

These diagrams clearly reveal two different emission processes. First, the data evidence the coherent emission which was predicted to occur from the "shortness" of the electron bunch [36]. This process is directly visible below the microbunching instability threshold [Fig. 3(a)]. The emission occurs as a few-period coherent THz pulses, without dynamical evolution from turn to turn. This corresponds to a quasiperfect Terahertz frequency comb [8,9].

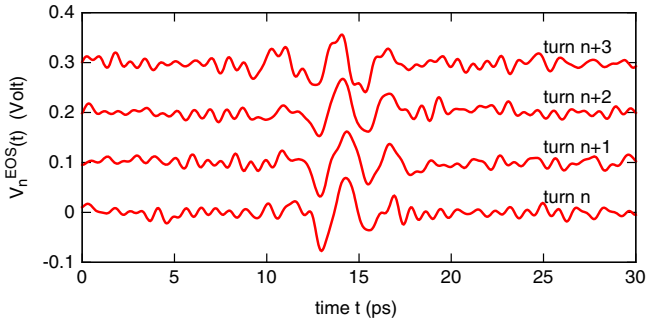

FIG. 2. Typical single-shot electro-optic sampling traces $V_n^{\mathrm{EOS}}(t)$ (corresponding to the THz CSR electric field emitted by one electron bunch, at four successive turns in the storage ring). The electron charge is 75 pC [second dot, i.e., bunch no. 65 on Fig. 1(b)]. For clarity, the signals are shifted vertically by 0.1 V.

A second process occurs when the charge exceeds the so-called microbunching instability threshold [Figs. 3(b), 3(c)]. An important part of the THz radiation is then emitted in the form of an oscillation, that drifts at each turn in the storage ring. This carrier-envelope phase drift stems from the appearance of microstructures, which are continuously moving inside the electron bunch, as described in the numerical simulations presented later. In addition, the first process, i.e., the coherent emission due to the bunch shortness, is expected to exist above the microbunching instability threshold. The signature of this contribution from the data presented in Figs. 3(b), 3(c) can be evidenced by computing the electric field pulse average over a large number of turns

$$V_{\mathrm{avg}}^{\mathrm{EOS}}(t) = \sum_{n=n0}^{n0+N-1} V_n^{\mathrm{EOS}}(t), \tag{1}$$

where $V_n^{\mathrm{EOS}}(t)$ is the electro-optic sampling signal of the THz pulses. This processing filters out the drifting component and may thus be viewed as a measure of the component due to the bunch shortness. This contribution $V_{\mathrm{avg}}^{\mathrm{EOS}}(t)$ (with $N \simeq 850$) is visible in Figs. 3(g), 3(h), 3(i). Note that this component is linked to the short-bunch mode operation, i.e., is not observed when long electron bunches are used [18,24].

From these data, it is also possible to reconstruct the turn-by-turn evolution of the THz pulse energy E_{THz}^n, with

$$E_{\mathrm{THz}}^n = \int_{t_1}^{t_2} |V_n^{\mathrm{EOS}}(t)|^2 dt, \tag{2}$$

where t_1 and t_2 are taken near the boundaries of the THz pulse. This signal corresponds to the signal that would be recorded with a standard "slow" detector [see Figs. 3(d)–3(f)]. It permits us to confirm in a very direct way that the modulation in the THz signal, which can be clearly seen in Fig. 3(e) and which had been observed in numerous studies [12,37–42], is directly related to the period of apparition of the microstructures in the bunch [Fig. 3(b)].

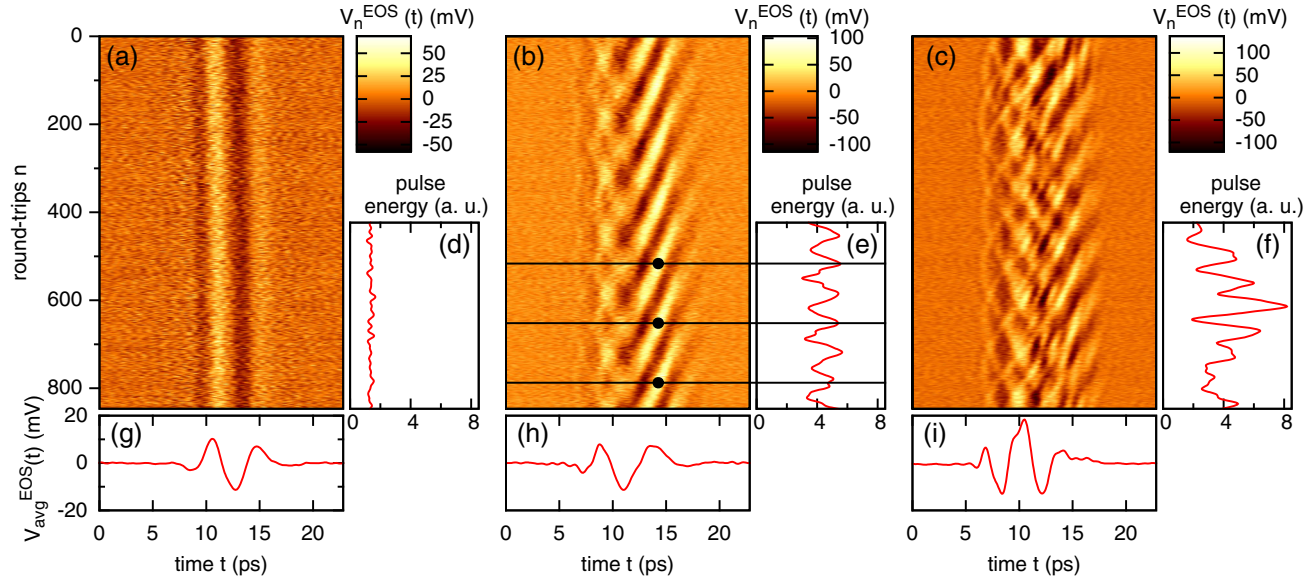

FIG. 3. (a)–(c) Terahertz pulses shapes [electro-optic sampling signal $V_n^{\mathrm{EOS}}(t)$] vs round-trips n in the storage ring. Below and above the microbunching instability threshold. Panels (a)–(c) correspond to bunch charges of $Q = 42$, 75, and 118 pC, respectively [i.e., bunch numbers 61, 65, and 92 in Fig. 1(b)]. Each horizontal cut corresponds to the electric field shape (as in Fig. 2). (d)–(f) Pulse energy versus turn number (integration over the time of the square of the EOS signal, and low-pass filtered at 50 kHz). Horizontal black lines and dots placed for visual guide. (g)–(i) Average electro-optic signal $V_{\mathrm{avg}}^{\mathrm{EOS}}(t)$. Note that the data (a) and (b) are recorded simultaneously (i.e., they correspond to a single oscilloscope recording).

We have then performed numerical integrations of analytic models, to make a comparison with these experimental data (obtained for the first time in a short-bunch mode), and also to access the 2D longitudinal phase space. We present here the results obtained with one of the most elementary models: the one-dimensional Vlasov-Fokker-Planck model with shielded CSR wakefield [17]. The evolution of the electron density is described by the phase space distribution $f(q,p,\theta)$, where θ is the time associated to the number of round-trips in the ring, and q and p are the longitudinal coordinate and electron energy variables, respectively. The dynamical evolution of $f(q,p,\theta)$ is determined by the following Vlasov-Fokker-Planck equation [17]:

$$\frac{\partial f(q,p,\theta)}{\partial\theta} - p\frac{\partial f}{\partial q} + \frac{\partial f}{\partial p}(q - I_c E_{wf}) = 2\epsilon\frac{\partial}{\partial p}\left(pf + \frac{\partial f}{\partial p}\right). \tag{3}$$

The time θ associated to round-trips is a dimensionless variable: $\theta = 2\pi f_s t$, where t is the time (in seconds) and f_s is the synchrotron frequency. The longitudinal position q and relative momentum p are the deviation from the so-called synchronous electron (with position z_0 and energy E_0). q and p are expressed in units of the equilibrium bunch length σ_z and energy spread σ_E at zero current: $q = (z - z_0)/\sigma_z$, and $p = (E - E_0)/\sigma_E$. $\epsilon = 1/(2\pi f_s \tau_s)$, where τ_s is the synchrotron damping time. $I_c = I(e2\pi R_c/2\pi f_s \sigma_E T_0)$, with I is the average beam current ($I = (Q/T_0)$), R_c the dipole radius of curvature, and T_0 the revolution period. All parameters are in MKS units.

The interaction between electrons is described by the term $E_{wf}(q,\theta)$ which represents the electron bunch wakefield (expressed in V/m, per Ampere of average current in the storage ring). We use here the CSR wakefield created by an electron bunch in a circular trajectory, between two parallel plates with distance $2h$. The exact expression of $E_{wf}(q,\theta)$ is well known [43], and detailed in Ref. [39]. Integration of Eq. (1) is performed using the semi-Lagrangian scheme, described in Ref. [44], and parameters are listed in the Fig. 4 caption.

Figure 4 shows the results of the numerical integration of Eq. (1) for three bunch charges $Q = 42$, 95, and 140 pC. We retrieve here qualitatively important features observed experimentally. Below the instability threshold, no microstructures are observable on the phase space [Fig. 4(a)] and the shape of the electron bunch is constant from turn to turn [Fig. 4(d)]. Just above the instability threshold, "branches" continuously appear on the bottom part of the phase space, and display a rotational motion at the synchrotron frequency [see Fig. 4(b) and the movie in the Supplemental Material [45]]. As a main consequence, the wakefield presents an oscillation which is drifting toward the bunch head [Fig. 4(e)]. For higher currents, the microstructures are more prominent [see Fig. 4(c) and the movie in the Supplemental Material [45]] and can reach the upper part of phase space. In this case, the wakefield [Fig. 4(f)] also presents an oscillation which is drifting toward the tail of the bunch (in addition to the oscillation drifting to the head).

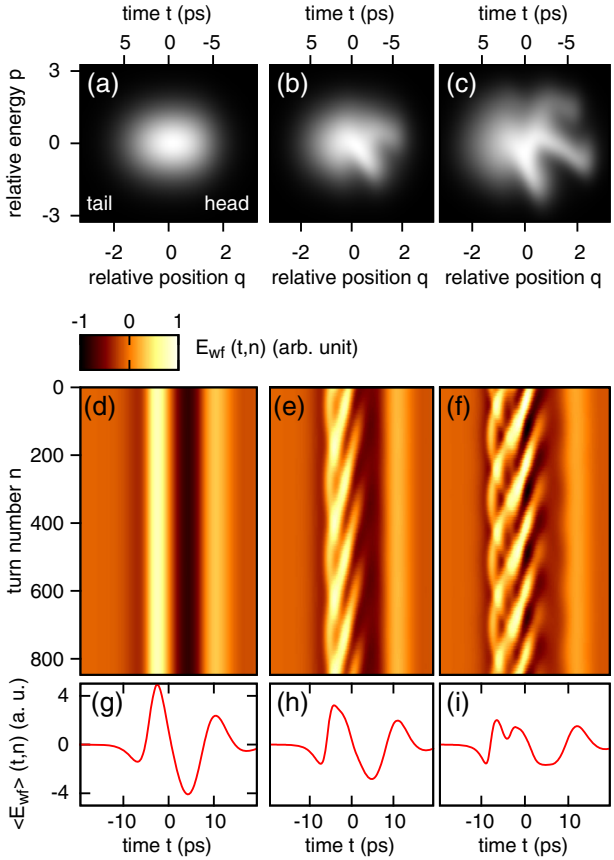

FIG. 4. Numerical simulations of the bunch dynamics, with a charge Q of 42, 95, and 140 pC, left, middle, and right column, respectively. (a)–(c) Electron distribution in the phase space (at the turn number $n = 0$). (d)–(f) Evolution of the electric field pulses (inside the chamber) $E_{wf}(t,n)$ vs turn number, with $t = -q\sigma_z/c$, $n = \theta/(2\pi f_s T_0)$, c the light velocity. (g)–(i) average over the turns of the emitted pulses. Simulation parameters: $E_0 = 2.75$ GeV, $f_s = 928$ Hz, $\sigma_E = E_0 \times 1.017 \times 10^{-3}$, $\sigma_z = 0.92$ mm, $\tau_s = 3.27$ ms, $R_c = 5.36$ m, $T_0 = 1.181$ μs, $h = 12.5$ mm. Measured average bunch length (rms) from numerical data: 3.25, 3.5, 3.9 ps for $Q = 42$, 95, and 140 pC, respectively.

We believe that the availability of this new type of data (CSR pulse shapes versus round-trips) is a precious tool for testing models of bunch dynamics (including wakefields), in a more clear-cut way than with classical means (i.e., average spectra, THz pulse energies, microbunching instability threshold, etc.). In the example presented here (where one of the most elementary model of wakefields is used), agreement as well as differences can clearly be seen. For the instance below threshold, the wakefield displays a longer period in the numerical simulation [Fig. 4(g)] than experimentally [Fig. 3(g)]. This may be attributed to differences in the impedance modeling (see, for example,

Ref. [46]) and/or in filter effects in the beam line which are not taken into account in the modeling. Differences at higher current are also perceptible, as experimental data [Fig. 3(c)] are more irregular than numerical ones [Fig. 4(f)]. We think that such comparisons of numerical and experimental diagrams can now be used as an important guide for the modeling process, including the crucial work of accelerator impedance modeling.

In conclusion, it is now possible to analyze in a complete way the coherent synchrotron radiation emission due to short electron bunches in storage rings. As a main result, we could directly visualize the predicted transition between a stable THz coherent emission (due to the "bunch shortness") and the emission due to the so-called microbunching instability. In the future, we believe that this viewing of CSR dynamics enables new and stringent tests for modeling the present and future storage ring facilities. In another perspective, these results show that THz spectra can be obtained at a MHz repetition rate, paving the way for ultrahigh repetition rate time-resolved THz spectroscopy.

We would like to thank Menlo Systems for important and the Synchrotron SOLEIL. The work has been supported by the Ministry of Higher Education and Research, Nord-Pas de Calais Regional Council and European Regional Development Fund (ERDF) through the Contrat de Projets État-Région (CPER photonics for society), by the CEMPI LABEX (ANR-11-LABX-0007), and by GENCI TGCC/IDRIS (i2015057057 and i2016057057).

*clement.evain@univ-lille1.fr

[1] G. L. Carr, S. L. Kramer, J. B. Murphy, R. P. S. M. Lobo, and D. B. Tanner, Observation of coherent synchrotron radiation from the NSLS VUV ring, Nucl. Instrum. Methods Phys. Res., Sect. A **463**, 387 (2001).

[2] M. Abo-Bakr, J. Feikes, K. Holldack, G. Wüstefeld, and H.-W. Hübers, Steady-State Far-Infrared Coherent Synchrotron Radiation detected at BESSY 2, Phys. Rev. Lett. **88**, 254801 (2002).

[3] J. M. Byrd, W. P. Leemans, A. Loftsdottir, B. Marcelis, M. C. Martin, W. R. McKinney, F. Sannibale, T. Scarvie, and C. Steier, Observation of Broadband Self-Amplified Spontaneous Coherent Terahertz Synchrotron Radiation in a Storage Ring, Phys. Rev. Lett. **89**, 224801 (2002).

[4] A. Mochihashi, M. Hosaka, M. Katoh, M. Shimada, and S. Kimura, Observation of THz synchrotron radiation burst in UVSOR-II electron storage ring, in *10th European Particle Accelerator Conference, Edinburgh, UK* (2006), THPLS042, p. 3380 (2006).

[5] E. Karantzoulis, G. Penco, A. Perucchi, and S. Lupi, Characterization of coherent THz radiation bursting regime at Elettra, Infrared Phys. Technol. **53**, 300 (2010).

[6] J. Barros *et al.*, Coherent synchrotron radiation for broadband terahertz spectroscopy, Rev. Sci. Instrum. **84**, 033102 (2013).

[7] B. E. Billinghurst, J. C. Bergstrom, C. Baribeau *et al.*, Observation of Wakefields and Resonances in Coherent Synchrotron Radiation, Phys. Rev. Lett. **114**, 204801 (2015).

[8] J. L. Steinmann *et al.*, Frequency-Comb Spectrum of Periodic-Patterned Signals, Phys. Rev. Lett. **117**, 174802 (2016).

[9] S. Tammaro, O. Pirali, P. Roy, J.-F. Lampin, G. Ducournau, A. Cuisset, F. Hindle, and G. Mouret, High density terahertz frequency comb produced by coherent synchrotron radiation, Nat. Commun. **6**, 7733 (2015).

[10] M. Abo-Bakr, J. Feikes, K. Holldack, P. Kuske, W. B. Peatman, U. Schade, G. Wüstefeld, and H.-W. Hübers, Brilliant, Coherent Far-Infrared (THz) Synchrotron Radiation, Phys. Rev. Lett. **90**, 094801 (2003).

[11] Y.-L. Mathis, B. Gasharova, and D. Moss, Terahertz radiation at ANKA, the new synchrotron light source in Karlsruhe, J. Biol. Phys. **29**, 313 (2003).

[12] J. Feikes, M. von Hartrott, M. Ries, P. Schmid, G. Wüstefeld, A. Hoehl, R. Klein, R. Müller, and G. Ulm, Metrology Light Source: The first electron storage ring optimized for generating coherent THz radiation, Phys. Rev. ST Accel. Beams **14**, 030705 (2011).

[13] I. P. S. Martin, G. Rehm, C. Thomas, and R. Bartolini, Experience with low-alpha lattices at the Diamond Light Source, Phys. Rev. ST Accel. Beams **14**, 040705 (2011).

[14] J. Barros *et al.*, Characteristics and development of the coherent synchrotron radiation sources for THz spectroscopy, J. Mol. Spectrosc. **315**, 3 (2015).

[15] S. Ahmed, J. Savolainen, and P. Hamm, Detectivity enhancement in THz electrooptical sampling, Rev. Sci. Instrum. **85**, 013114 (2014).

[16] G. Stupakov and S. Heifets, Beam instability and microbunching due to coherent synchrotron radiation, Phys. Rev. ST Accel. Beams **5**, 054402 (2002).

[17] M. Venturini and R. Warnock, Bursts of Coherent Synchrotron Radiation in Electron Storage Rings: A Dynamical Model, Phys. Rev. Lett. **89**, 224802 (2002).

[18] E. Roussel *et al.*, Microbunching Instability in Relativistic Electron Bunches: Direct Observations of the Microstructures Using Ultrafast YBCO Detectors, Phys. Rev. Lett. **113**, 094801 (2014).

[19] I. Katayama *et al.*, Electric field detection of coherent synchrotron radiation in a storage ring generated using laser bunch slicing, Appl. Phys. Lett. **100**, 111112 (2012).

[20] F. Müller, P. Peier, V. Schlott, B. Steffen, T. Feurer, and P. Kuske, Electro-optical measurement of sub-ps structures in low charge electron bunches, Phys. Rev. ST Accel. Beams **15**, 070701 (2012).

[21] N. Hiller, A. Borysenko, E. Hertle *et al.*, Single-shot electro-optical diagnostics at the ANKA storage ring, *Proceedings of the Beam Instrumentation Conference, Monterey, CA, USA* (2014), MOPD17.

[22] F. Coppinger, A. S. Bhushan, and B. Jalali, Photonic time stretch and its application to analog-to-digital conversion, IEEE Trans. Microw. Theory Techn. **47**, 1309 (1999).

[23] K. Goda and B. Jalali, Dispersive Fourier transformation for fast continuous single-shot measurements, Nat. Photonics **7**, 102 (2013).

[24] E. Roussel *et al.*, Observing microscopic structures of a relativistic object using a time-stretch strategy, Sci. Rep. **5**, 10330 (2015).

[25] A. Mahjoubfar, C. L. Chen, and B. Jalali, Design of warped stretch transform, Sci. Rep. **5**, 17148 (2015).
[26] L. Chen, A. Mahjoubfar, and B. Jalali, Context-aware image compression, PLoS One **10**, e0125106 (2016).
[27] C. L. Chen, A. Mahjoubfar, L.-C. Tai, I. K. Blaby, A. Huang, K. R. Niazi, and B. Jalali, Deep Learning in Label-free Cell Classification, Sci. Rep. **6**, 21471 (2016).
[28] J. Savolainen, S. Ahmed, and P. Hamm, Two-dimensional Raman-terahertz spectroscopy of water, Proc. Natl. Acad. Sci. U.S.A. **110**, 20402 (2013).
[29] B. Miriam *et al.*, Fast mapping of terahertz bursting thresholds and characteristics at synchrotron light sources, Phys. Rev. Accel. Beams **19**, 110701 (2016).
[30] M.-A. Tordeux, J. Barros, A. Bence *et al.*, Low-alpha operation for the SOLEIL storage ring, *2012 International Particle Accelerator Conference, IPAC12* 1608 (2012).
[31] C. Szwaj, C. Evain, M. Le Parquier, P. Roy, L. Manceron, J.-B. Brubach, M.-A. Tordeux, and S. Bielawski, High sensitivity photonic time-stretch electro-optic sampling of terahertz pulses, Rev. Sci. Instrum. **87**, 103111 (2016).
[32] Z. Jiang and X.-C. Zhang, Electro-optic measurement of THz field pulses with a chirped optical beam, Appl. Phys. Lett. **72**, 1945 (1998).
[33] I. Wilke, A. M. MacLeod, W. A. Gillespie, G. Berden, G. M. H. Knippels, and A. F. G. van der Meer, Single-Shot Electron-Beam Bunch Length Measurements, Phys. Rev. Lett. **88**, 124801 (2002).
[34] B. Steffen *et al.*, Electro-optic time profile monitors for femtosecond electron bunches at the soft x-ray free-electron laser FLASH, Phys. Rev. ST Accel. Beams **12**, 032802 (2009).
[35] J. Wong *et al.*, Photonic time-stretched analog-to-digital converter amenable to continuous-time operation based on polarization modulation with balanced detection scheme, J. Lightwave Technol. **29**, 3099 (2011).
[36] F. Sannibale *et al.*, A Model Describing Stable Coherent Synchrotron Radiation in Storage Ring, Phys. Rev. Lett. **93**, 094801 (2004).
[37] P. Kuske, Investigation of the temporal structure of CSR-bursts at BESSY II, in *Proceedings of PAC09, Vancouver, BC, Canada* (2009), FR5RFP063, 4682.
[38] C. Evain *et al.*, Spatio-temporal dynamics of relativistic electron bunch during the micro-bunching instability in storage rings, Europhys. Lett. **98**, 40006 (2012).
[39] E. Roussel, C. Evain, C. Szwaj, and S. Bielawski, Micro-bunching instability in storage rings: Link between phase-space structure and terahertz coherent synchrotron radiation radio-frequency spectra, Phys. Rev. ST Accel. Beams **17**, 010701 (2014).
[40] V. Judin, N. Hiller, A. Hofmann *et al.*, Spectral and temporal observations of CSR at ANKA, *2012 International Particle Accelerator Conference (IPAC12), New Orleans, USA* (2012), p. 1623.
[41] R. Bartolini, G. Cinque, I. Martin, G. Rehm, and C. Thomas, CSR and THz emission measurements at the diamond light source, *2011 International Particle Accelerator Conference (IPAC11)* (2011), THPC068, p. 3050.
[42] B. E. Billinghurst, J. C. Bergstrom, C. Baribeau, T. Batten, T. E. May, J. M. Vogt, and W. A. Wurtz, Longitudinal bunch dynamics study with coherent synchrotron radiation, Phys. Rev. Accel. Beams **19**, 020704 (2016).
[43] J. B. Murphy, S. Krinsky, and R. L. Gluckstern, Longitudinal wakefield for an electron moving on a circular orbit, Part. Accel. **57**, 9 (1997).
[44] R. L. Warnock and J. A. Ellison, SLAC PUB Report No. 8404, 2000.
[45] See Supplemental Material at http://link.aps.org/supplemental/10.1103/PhysRevLett.118.054801 for the movie corresponding for Fig. 4.
[46] A. D. Garg, S. Yadav, M. Kumar, B. B. Shrivastava, A. K. Karnewar, A. Ojha, and T. A. Puntambekar, Studies of longitudinal profile of electron bunches and impedance measurements at Indus-2 synchrotron radiation source, Nucl. Instrum. Methods Phys. Res., Sect. A **814**, 66 (2016).